Organic Electronics 12 (2011) 1159–1165

Contents lists available at ScienceDirect

Organic Electronics

journal homepage: www.elsevier.com/locate/orgel

Letter

Effects of the PEDOT interface trap distribution in polymeric OLEDs

Mario Petrosino *, Alfredo Rubino

Dipartimento di Ingegneria dell'Informazione ed Ingegneria Elettrica, Università degli Studi di Salerno, Via Ponte don Melillo 1, 84084 Fisciano (SA), Italy

ARTICLE INFO

Article history:
Received 5 July 2010
Received in revised form 23 March 2011
Accepted 29 March 2011
Available online 11 April 2011

Keywords:
OLED
Admittance spectra
Interface trap distribution

ABSTRACT

Four kinds of commercial PEDOT dispersions have been used to realize ITO/PEDOT/PF6/Al polymeric OLEDs. The effects of the different PEDOT layers have been analyzed by the means of static current–voltage characterizations and admittance spectra. The measurements have revealed a good agreement with the Nicollian–Brews model returning the density of the interface traps; moreover the role of the trapping rate has been focused in terms of density of carriers available for the conduction.

1. Introduction

During the last 10 years lots of studies have been performed about the physics of Organic Light Emitting Diodes (OLEDs). In this kind of device the Conductive Polymers (CPs) show relevant importance because of their capability as carrier injector together other electro-optical properties. In particular between the anode electrode – usually Indium Tin Oxide (ITO) – and the Hole Transporting Layer (HTL), polymeric or molecular, an hole injection layer realized by the means of a conductive polymer is interposed. The improvement of the charge injection is related to the work functions of anode, HTL and of the interposed CP; the latter work function is chosen as intermediate value between the other two [1–5], obtaining a lower hole potential barrier into the OLED and then a higher carriers injection. The most used CP is the PEDOT:PSS, a blend of thiophene-based molecules and polystyrene based polymers – Poly(3,4-EthyleneDiOxyThiophene):Poly(StyreneSulfonate), showing good electrical conductivity, good light transparency into the visible range, work function similar to gold one (about 5 eV) and finally a good solubility in water. The insertion of PEDOT:PSS between anode and HTL layers, besides increasing charge injection, preserves the device from the fast degradation occurring when these layers are put in direct contact. These two effects have a relevant consequence on the device behaviour, because they contribute to the OLED voltage threshold reduction and to the increment of the electro-optical efficiency.

PEDOT:PSS [6–19], known actually as Clevios™ P (its commercial name has been Baytron® P until 2008), is distributed in several kinds of dispersions, differing mainly for: constituents ratio, impurity density, kind of dopant and dispersion solvent. Since all these parameters tune the PEDOT work function and conductivity [20], the particular PEDOT dispersion employed into the OLED plays a crucial role in the device electro-optical behaviour [15] but the physical mechanisms of these phenomena are not well understood yet. In this work the authors propose an interpretation of the physics of the anode interface barrier in terms of intra-gap state distribution and trapping rate by the means of admittance spectra measurements of ITO/PEDOT/PF6/Al OLEDs, where PF6 means poly(9,9-dihexyl-9H-fluorene-2,7-diyl).

2. Experimental

Commercial ITO (200 nm thick) coated glass substrates were used as transparent conductive anode. Moisture and carbon impurities have been removed from the ITO surface by the means of HCl baths [21,22]. In order to build contact

* Corresponding author. Fax: +39 089 962815.
E-mail address: mpetrosino@unisa.it (M. Petrosino).

1566-1199/$ - see front matter © 2011 Elsevier B.V. All rights reserved.
doi:10.1016/j.orgel.2011.03.044

areas and to prevent the formation of shorts during the top electrode contact soldering, the ITO layers were patterned by a photolithographical process. Four kinds of ITO/PEDOT/PF6/Al OLEDs – denoted as *A*, *B*, *C* and *D* – were manufactured employing four commercial PEDOT dispersions: Clevios™ P CH 8000 (previously known as Baytron® P 8000), a dispersion with PEDOT:PSS ratio 1:20 (w/w) for the *A* device; Clevios™ P AI 4083 (previously known as Baytron® P 4083), a dispersion with PEDOT:PSS ratio 1:6 (w/w) for the *B* device; a poly(3,4-ethylenedioxythiophene)-*block*-poly(ethylene glycol) – PEDOT–PEG – dispersion with *p*-toluenesulfonate (PTS) as dopant for the *C* device; a PEDOT–PEG dispersion with perchlorate (PC) as dopant for the *D* device. The dispersions characteristics and the deposition parameters are summarised in Table 1. For all the devices the PEDOT layer is 70 nm thick. After the PEDOT coating, the devices were completed with the same following steps: the obtained films were backed under nitrogen flow at 120 °C for 15 min and then PF6 was spun over the PEDOT layer at 1500 rpm from a 1.0% (w/w) chlorobenzene solution obtaining a thickness of 90 nm. After the deposition the samples were backed in vacuum at 50 °C for 3 h. Finally, the OLED structure was completed with a 200 nm thick Al layer deposited by thermal evaporation with a base pressure of 10^{-7} mbar. The active device area is 12.6 mm^2 and the final realized structure is shown into the inset of Fig. 1. Electrical analysis was performed by the means of a HP 4192A impedance analyzer and a Keithley 4200 semiconductor parameter analyzer under ambient condition.

3. Results and discussion

In Fig. 1 typical current density–voltage characteristics are shown; both the devices realized using PEDOT–PEG (C and D) are more conductive than those realized using PEDOT:PSS, and the most conductive one is that realized with a layer doped with perchlorate (D device). Comparing the results shown in Fig. 1 and Table 2 an anomalous behaviour can be observed: the device current increases with the anode potential barrier. In fact, as shown into the inset of Fig. 1, since the ITO work function is 4.8 eV and the PF6 HOMO level is 5.8 eV, reducing the PEDOT work function from 5.2 to 4.2 eV an increase of the PEDOT/PF6 hole barrier is awaited, with the effect of a reduction of the number of injected holes and therefore a reduction of the device current. Instead, the experimental results show an opposite behaviour suggesting the presence of other dominant phenomena into the device about the charge injection and transport. Capacitance-frequency and conductance-frequency measurements have been performed at various biases for all the devices and, as shown in Fig. 2 (for simplicity only for device A), these spectra don't vary with the applied voltage below the optical threshold. The bias independent capacitance is a known result tuned by charge phenomena, and it is well analyzed in literature [23]. In order to analyze the device in the under-threshold regime, we have performed all the admittance spectra at 0 V bias.

The spectra reported in Fig. 3 show capacitances having decreasing monotonic behaviour with low frequency unitary value of about 21 nF/cm^2 for the first three kinds of device and 48 nF/cm^2 for the D one. The Fig. 4 show the loss (L) spectra defined as

$$L = \frac{G}{\omega} \tag{1}$$

where G is the electrical conductance and ω the angular frequency of the applied signal: the devices A, B and C have one loss-peak while the D device shows two peaks. The loss-peak specifies the relaxation time constant (τ): 220 ns, 290 ns and 2.31 μs for A, B, C, respectively, while the device D has a low frequency peak with a time constant of 160 μs and a high frequency one of 140 ns. In literature [24] it is reported an experiment similar to ours where the authors study OLED devices with a similar structure, ITO/PEDOT:PSS/PF8/cathode, but with different PF8 layer thicknesses. The results of their measurements show an unexplained thickness dependence of the relaxation time. Our spectral results can be interpreted by a physical key shown in literature [25–31]: it is known that a semiconductor junction shows peaks in Loss vs. Frequency diagram when a trap distribution is at the semiconductor interface. In the case of a single energy level, Nicollian and Brews [32] proved that the device conductance and capacitance are described by the following equations

$$\frac{G}{\omega} = \frac{qD_S\omega\tau}{1+(\omega\tau)^2} \tag{2}$$

$$C_S = \frac{qD_S}{1+(\omega\tau)^2} \tag{3}$$

where C_S is the capacitance, q is the electron charge, D_S is the interface state density and τ is the time constant. For a distribution of more close energy trap levels [32], the device admittance is described by

$$\frac{G}{\omega} = \frac{qD_S}{2\omega\tau}\ln\left[1+(\omega\tau)^2\right] \tag{4}$$

$$C_S = \frac{qD_S}{\omega\tau}tan^{-1}(\omega\tau) \tag{5}$$

Table 1
Technological parameters of the PEDOT layers.

	PEDOT dispersion	Constituent ratio	Solution	Dopant	Deposition rate and time
A	PEDOT:PSS	1:20	3 wt.% in water	None	2000 rpm for 30 s
B	PEDOT:PSS	1:6	1.7 wt.% in water	None	2000 rpm for 20 s
C	PEDOT–PEG	1:1	1 wt.% in nitromethane	p-toluenesulfonate (PTS)	1000 rpm for 30 s
D	PEDOT–PEG	1:1	1 wt.% in perchlorate	Perchlorate (PC)	1000 rpm for 30 s

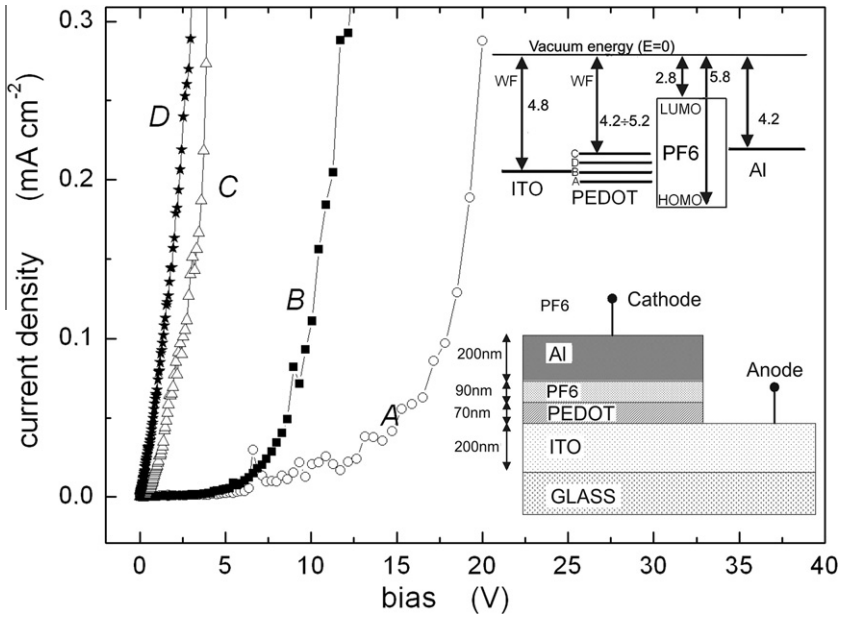

Fig. 1. Current–voltage characteristics of the polymeric OLEDs realized at different PEDOT dispersions. In the upper inset the energetic diagram of the realized samples where the PF6 HOMO and LUMO, and the ITO, PEDOT and Al work functions are drawn: the devices differ only for the kind of PEDOT dispersion with a variation in work function between 4.2 and 5.2 eV. In the lower inset the devices structure (the figure is not in scale).

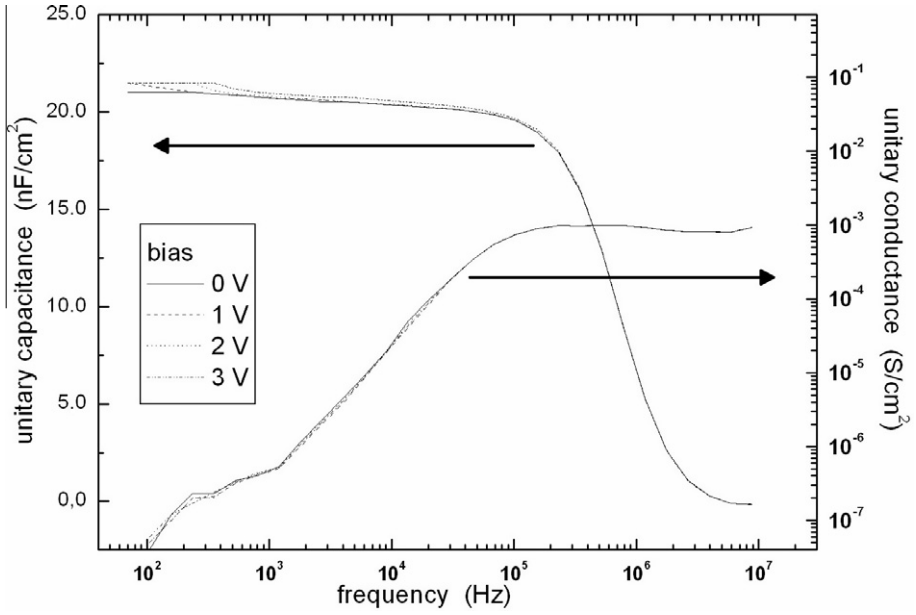

Fig. 2. Typical unitary capacitance and conductance spectra at different biases (for simplicity only the A device measurements are shown). For all A, B, C, D devices the spectra do not change with bias.

The Nicollian and Brews model was developed to study the trap effect in MOS Field Effect Transistor, but it has also been used in the analysis of the interface state distribution in MIS structure (Metal/Insulator/Semiconductor) and in particular for organic and inorganic diodes [33–36].

For each device, besides the time constant τ, we have extracted the interface state density D_S from the peaks in Fig. 4, as reported in Table 2. In Figs. 3 and 4 the continuous lines represent the Eqs. 2,3,4,5, drawn using the experimental estimation of D_S and τ. As it can be seen, a good agreement between the experimental data and the single energy level model (Eqs. 2 and 3) is obtained for the devices A, B, C and the high frequency peak of D (denoted with *c* in Figs. 3 and 4). The low frequency peak of device

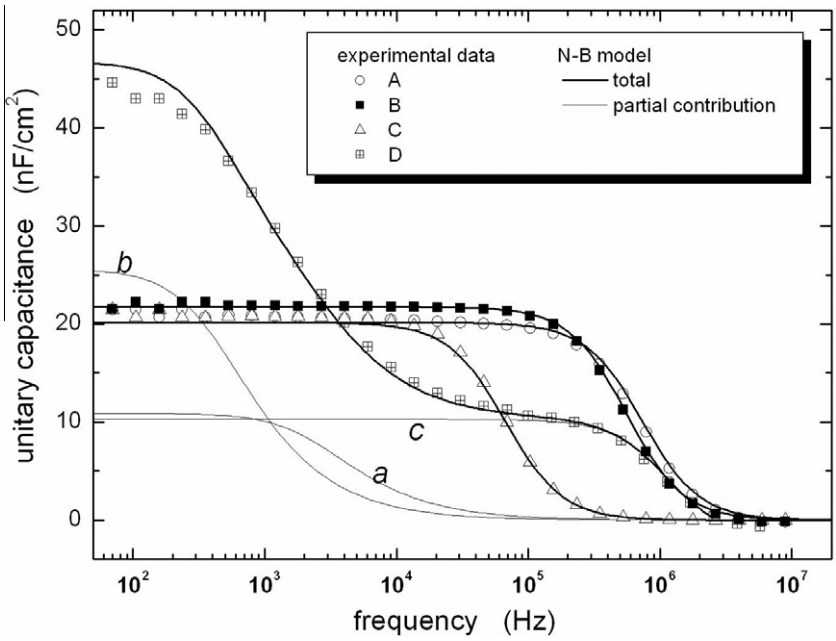

Fig. 3. Unitary capacitance spectra of the polymeric OLEDs. Decays with single time constant are visible in the figure for the A, B, C devices while a decay with a double time constant is evident for the D device.

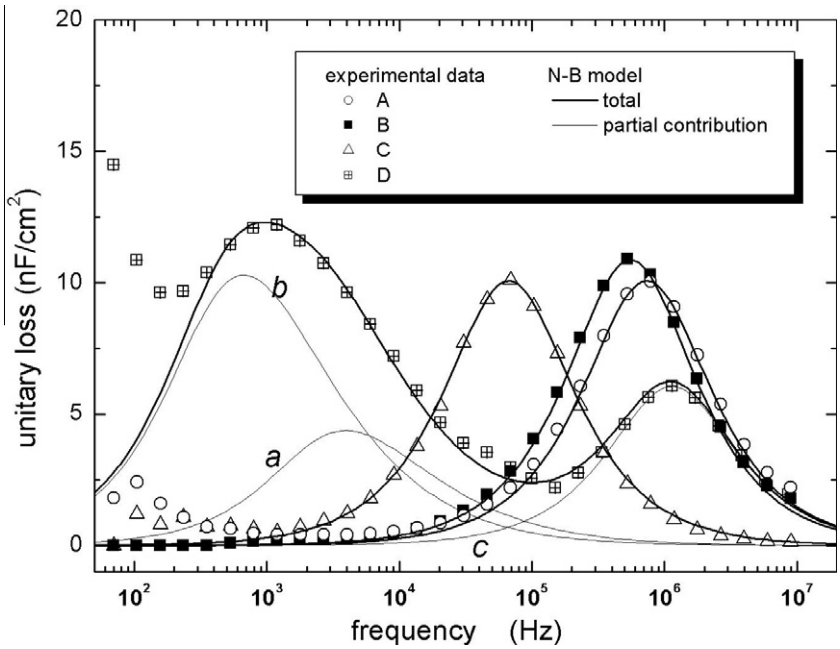

Fig. 4. Unitary loss spectra (G/ω) of the devices. A single peak spectra are visible in the figure for A, B, C devices while a double peak spectrum is evident for the D device.

D results to be the sum of two multiple-level distributions (denoted with *a* and *b* in Figs. 3 and 4) modelled by Eqs. 4, 5. The results confirm the model applicability in our case. Because the devices vary exclusively for the kind of PEDOT, the differences in admittance measurements are only imputable to this layer: in other words, the found variability between the four interface trap distributions is only ascribable to the four different PEDOT dispersions. As proposed in [41], the curves shown in Fig. 4 can be interpreted also as the effect of both interface and bulk trap distributions: in fact the low frequency peak can be ascribed to interface phenomena while the high frequency one is

usually due to bulk traps. Considering the Brunson interpretation [41] only in *D* device the bulk traps have a prominent effect. However, as pointed out by Lang [42], the capacitance measurements experience mainly the interface states, being their spatial sensitivity higher at the interface and decreasing towards bulk material [25].

As indicated above, A and B devices differ only for the PEDOT:PSS ratio determining two similar interface state distributions. The C device differs from the D only for the dopant (both are PEDOT–PEG block-copolymers), resulting in different defect state distribution; the time constant of the C device is similar to those of the A and B ones, while, for the D device, the higher frequency time constant is lower than those of the A and B devices, the two lower frequency time constants cannot be compared the other ones. As described in [25,26] the relaxation time τ can be described by the following energetic law (Arrhenius)

$$\omega_R = \frac{1}{\tau} = A_t e^{-\Delta E/k_B T} \tag{6}$$

where A_t is a material constant, ΔE is the energy deep of the state respect the band edge, k_B is the Boltzmann constant and T the absolute temperature. The hole anode barrier φ_i (for the *i*-device) can be indicated respect to one of the four kinds of device. Choosing A device as reference, we can write

$$\varphi_i = \varphi_A + \Delta\varphi_i \tag{7}$$

The total current density in every point of the device is constant. The current density at the PEDOT/PF6 junction, neglecting the electron current, can be written as the product between the holes concentration (p) and the probability of the barrier crossing (Boltzmann law), obtaining

$$J(V_{app}) = Kqp\mu_{PEDOT_i} e^{\gamma V_{app}} e^{\beta\varphi_i} = K\sigma_{PEDOT_i} e^{\gamma V_{app}} e^{\beta\varphi_i} \tag{8}$$

similar to the classical p–n junction equation. The constant K collects all the effects not ascribable to the PEDOT, μ_{PEDOT_i} is the hole mobility of the PEDOT layer, V_{app} is the applied bias, γ and β are the exponential factors related to the anode hole barrier, considered independent from the particular kind of device and finally, σ_{PEDOT_i} is the bulk conductivity of the *i* PEDOT layer.

In order to remove the effect of the PEDOT conductivity, we can divide Eq. 8 for σ_{PEDOTi}

$$\frac{J(V_{app})}{\sigma_{PEDOT_i}} = Ke^{\gamma V_{app}} e^{\beta\varphi_i} \tag{9}$$

obtaining the curves J/σ shown in Fig. 5 as function of the hole anode barrier variation $\Delta\varphi_i$ (respect to the A device) at various biases. This values follow linear behaviours for many bias voltages in a semi-log plot (except for C device which values are out of liner trend): this result suggests that the exponential dependence (at fixed temperature) on φ_i described in Eq. 8 is verified. Moreover, the slopes in Fig. 5 are different for each bias value: this result suggests that the β factor is bias dependent, but the purpose of this work is only to point out that the experimental points of Fig. 5 follows linear trends. In order to explain why the values extracted from the current–voltage characteristic of the C device do not follow the behaviour predict by Eq. 8 or Eq. 9, other phenomena have to be taken into account. The exception of the *C* device can be justified considering the different trap time constants and in particular the lower τ of the device (dominant τ). As described in [25,26] the time constant is related to the carrier capture rate c_c

$$\tau = \frac{2\pi}{c_c} \tag{10}$$

When the applied signal frequency ω is less than $1/\tau$, the traps can follow the voltage variations by the means of the emission and capture processes. Instead, for $\omega > 1/\tau$, only the untrapped charge can respond to the voltage variations giving rise to a decrement of the device capacitance and the slope of the conductance. This implies that the maximum of the normalized conductance (loss) is at $\omega = 1/\tau$, in other words at the resonance pulsation of the trapping phenomenon. From Eqs. 6 and 10 the increment of τ gives rise to a decrement of the capture rate resulting in a higher fraction of untrapped carriers available for the conduction. From Table 2, the devices A, B and D show a similar dominant τ ($140 \div 290$ ns) and so they have trap distributions with similar energetic depth. Instead the C device shows a greater dominant τ (2.31 μs), then a deeper trap distribution (a higher energy gap), that allows an higher fraction of carriers available for the conduction, for this reason the J/σ values for the device C are higher then for the other devices. The plot of Fig. 5 help us to understand also the previous reported anomaly about the current increment with the hole anode barrier (see Fig. 1 and Table 2): in fact, in Fig. 5 we can see how the current density normalized through the conductivity decreases increasing the anode hole barrier, as expected. Considering Fig. 1, where the current–voltage characterises are reported, we have to take account of the effects of the different PEDOT conductivities that have a fundamental role in the device electrical behaviour.

Table 2
Electrical and energetical properties of the PEDOT layers and interfaces.

Device/ distribution	Energy distribution	PEDOT work function (eV)	PEDOT conductivity σ $(\Omega\,\mathrm{cm})^{-1}$	State density D_S $(\mathrm{eV}^{-1}\,\mathrm{cm}^2) \times 10^{11}$	Time constant τ $(\mathrm{s}) \times 10^{-6}$
A	Single level	5.15 [20]	5×10^{-6} [40]	1.26	0.22
B	Single level	4.85 [20]	2×10^{-4} [37]	1.36	0.29
C	Single level	4.19 [38]	1×10^{-3} [39]	1.26	2.31
D (a)	Multiple levels	4.33 [38]	0.4 [39]	0.68	80.4
D (b)	Multiple levels			1.62	4.71
D (c)	Single level			0.76	0.14

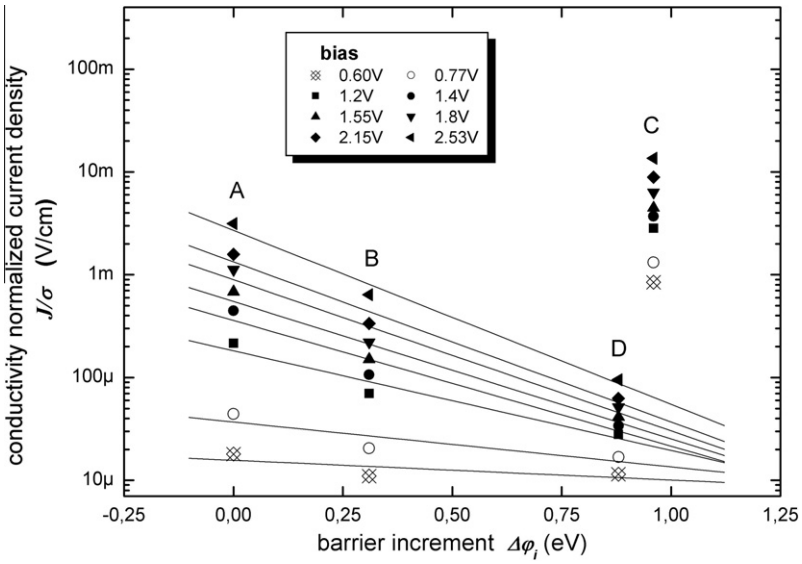

Fig. 5. Normalized current densities (J/ω) as function of the anode hole barrier increment (respect to the PEDOT work function of the A device) at different voltage biases. Only the C device does not follow the linear trend in the semi-log plot.

4. Conclusions

The analysis of polymeric OLEDs varying only for the kind of PEDOT dispersion has allowed to ascribe the variations of the admittance spectra to the effects of interface trap distribution: a good agreement between the experimental data and the Nicollian–Brews model has been found. The exponential dependence of the current on the hole barrier height has been verified only for three kinds of devices; the exception of the fourth has been explained in terms of trapping rate that tunes the increment of the number of carriers available for the conduction. The study of the normalized current has allow to evidence the importance of the PEDOT conductivity of the layer, often forgotten to advantage of consideration about the energetic levels of the layers work functions.

Acknowledgments

Support by the PHONEMA project financed by the *Ministero dell'Università e della Ricerca (MIUR)* in the ambit of the *Futuro in Ricerca* program is gratefully acknowledged.

The authors thank the precious and fundamental aid of Dr. Paolo Vacca (at the time with Portici ENEA Research Centre) in the fulfilment of the experimental part of this work.

References

[1] P.A. Lane, P.J. Brewer, J. Huang, D.D.C. Bradley, J.C. deMello, Phys. Rew. B 74 (2006) 125320.
[2] P.J. Brewer, J. Huang, P.A. Lane, A.J. deMello, D.D. Bradley, J.C. deMello, Phys. Rew. B 74 (2006) 115202.
[3] A. van Dijken, A. Perro, E.A. Meulenkamp, K. Brunner, Org. Electr. 4 (2003) 131.
[4] H.S. Woo, R. Czerw, S. Webster, D.L. Carroll, J.W. Park, J.H. Lee, Synth. Met. 116 (2001) 369.
[5] A.C. Arias, M. Granstrom, K. Petrisch, R.H. Friend, Synth. Met. 102 (1999) 953.
[6] S.W. Tsang, S.C. Tse, K.L. Tong, S.K. So, Org. Electr. 7 (2006) 474.
[7] C. Carlberg, X. Chen, O. Inganas, Solid State Ionics 85 (1996) 73.
[8] H.S. Kang, J.W. Lee, M.K. Kim, J. Joo, J.M. Ko, J.Y. Lee, J. Appl. Phys. 100 (2006) 064508.
[9] J. Yang, D.C. Martin, Sens. Actuators, A 113 (2004) 204.
[10] K.Z. Xing, M. Fahlman, X.W. Chen, O. Inganas, W.R. Salanek, Synth. Met. 89 (1997) 161.
[11] K. Lota, V. Khomenko, E. Frackowiak, J. Phys. Chem. Solids 65 (2004) 295.
[12] D. Wakizaka, T. Fushimi, H. Ohkita, S. Ito, Polymer 45 (2004) 8561.
[13] H.S. Kang, H.-S. Kang, J.K. Lee, J.W. Lee, J. Joo, J.M. Ko, M.S. Kim, J.Y. Lee, Synth. Met. 155 (2005) 176.
[14] G. Sonmez, P. Schottland, J.R. Reynolds, Synth. Met. 155 (2005) 130.
[15] P. Vacca, M. Petrosino, R. Miscioscia, G. Nenna, C. Minarini, D. Della Sala, A. Rubino, Thin Solid Films 516 (2008) 4232.
[16] H.J. Snaith, H. Kenrick, M. Chiesa, R.H. Friend, Polymer 46 (2005) 2573.
[17] Liqiang Li, M. Hirtz, W. Wang, Chuan Du, H. Fuchs, Lifeng Chi, Adv. Mater. 22 (2010) 1374.
[18] H. Okuzaki, Y. Harashina, H. Yan, Eur. Polym. J. 45/1 (2009) 256.
[19] E. Vitoratos, S. Sakkopoulos, E. Dalas, N. Paliatsas, D. Karageorgopoulos, F. Petraki, S. Kennou, S.A. Choulis, Org. Electr. 10/1 (2009) 61.
[20] N. Koch, A. Elschener, J.P. Rabe, R.L. Johnson, Adv. Mater. 17 (2005) 330.
[21] P. Vacca, M. Petrosino, A. Guerra, R. Chierchia, C. Minarini, D. Della Sala, A. Rubino, J. Phys. Chem. C 111 (2007) 17404.
[22] P. Vacca, M. Petrosino, R. Chierchia, A. Guerra, C. Minarini, A. Rubino, Macromol. Symp. 247 (2007) 333.
[23] Vishal Shrotriya, Yang Yang, J. Appl. Phys. 97 (2005) 054504.
[24] T. Okachi, T. Nagase, T. Kobayashi, H. Naito, Thin Solid Films 517 (2008) 1327.
[25] D.V. Lang, J.D. Cohen, J.P. Harbison, Phys. Rev. B 25 (8) (1982) 5285.
[26] J.D. Cohen, D.V. Lang, Phys. Rev. B 25 (8) (1982) 5321.
[27] S.S. Hegedus, E.A. Fagen, IEEE Trans. Electr. Dev. 39 (10) (1992) 2368.
[28] S.S. Hegedus, E.A. Fagen, J. Appl. Phys. 71 (12) (1992) 5941.
[29] I. Balberg, E. Gal, J. Appl. Phys. 58 (7) (1985) 2617.
[30] D. Jousse, S. Deleonibus, J. Appl. Phys. 54 (7) (1983) 4001.
[31] A. Khan, J. Woollam, Y. Chung, B. Banks, Electr. Dev. Lett. 4 (5) (1983) 146.
[32] E.H. Nicollian, J.R. Brews, MOS Physics and Technology, J. Wiley & Sons, 2003.
[33] M. Yun, R. Ravindran, M. Hossain, S. Gangopadhyay, U. Scherf, T. Bünnagel, F. Galbrecht, M. Arif, S. Guhaa, Appl. Phys. Lett. 89 (2006) 013506.
[34] R. Sahingoz, H. Kanbur, M. Voigt, C. Soykan, Synth. Met. 158 (2008) 727–731.
[35] A. Azim Khan, J.A. Woollam, Y. Chung, B. Banks, IEEE Electr. Dev. Lett. 4 (5) (1983) 146–149.

[36] D.T. Simon, M.S. Griffo, R.A. DiPietro, S.A. Swanson, S.A. Carter, Appl. Phys. Lett. 89 (2006) 133510.
[37] T. Sakurai, M. Nishiyama, Y. Nishioka, H. Kobayashi, Appl. Phys. Lett. 81 (2) (2002) 271.
[38] Y. Mochizuki, M. Mizuta, Appl. Phys. Lett. 69 (20) (1996) 3051.
[39] S. Sapp, S. Luebben, Y.B. Losovyj, P. Jeppeson, D.L. Schulz, A.N. Caruso, Appl. Phys. Lett. 88 (2006) 152107.
[40] M. Petrosino, P. Vacca, R. Miscioscia, G. Nenna, C. Minarini, A. Rubino, Proc. SPIE 6593 (2007) 659310–659311.
[41] K.M. Brunson, D. Sands, C.B. Thomas, H.S. Reehal, J. Appl. Phys. 62 (1) (1987) 185–189.
[42] D.V. Lang, in: P. Bräunlich (Ed.), Space Charge Spectroscopy in Semiconductors in Thermally Stimulated Relaxation In Solids, Springer-Verlag, USA, 1979.